13th International Symposium on Turbulence and Shear Flow Phenomena (TSFP13)
Montreal, Canada, June 25–28, 2024

ROUGHNESS IMPACTS ON BOUNDARY LAYER SUPERSTRUCTURES

Humza Butt, Bhavika Sharma, Shishir Damani, Eric Totten, Todd K. Lowe, William J. Devenport
Kevin T. Crofton Department of Aerospace and Ocean Engineering
Virginia Polytechnic Institute and State University
Blacksburg, VA 24061
hbutt@vt.edu

ABSTRACT

Momentum transport within a turbulent boundary layer in the vicinity of rough and smooth walls is discussed in the context of their contributions to inducing wall pressure fluctuations. Specifically, the existence and nature of turbulent superstructures, in the presence of ordered surface roughness is presented. Results obtained from wall-parallel stereoscopic Particle Image Velocimetry (PIV) show evidence of streamwise-oriented meandering coherent motions convecting downstream with the boundary layer over both smooth and rough surfaces. Statistical analyses conducted at friction Reynolds number (Re_τ) ≈ 3300 (smooth) and 6200 (rough), at a near-zero pressure gradient are presented. The presence of roughness limits the streamwise extent of coherence in u velocity, while reorganizing the streamwise momentum into wall-normal components. While insignificant impacts in the spanwise component are reported, the relative importance of the slow terms in the pressure Poisson equation are highlighted by showing the extent of their coherence within the measurement domain. The need for increased number of flow run-through times is also suggested for improved statistical convergence.

INTRODUCTION

Large-scale organized motions in the vicinity of an aerodynamic surface have been a topic of interest, specifically for the fluid mechanics and the aeroacoustics community. It is hypothesized that the large-scale coherent motions may be responsible for the generation of low-wavenumber surface pressure fluctuations in surfaces that interact with turbulence. This drives a particular interest in the investigation of superstructures as they may generate both near and far-field disturbances in the velocity and pressure field.

The idea of the existence of organized motions larger than the boundary layer thickness δ was speculated by Kovasznay (1970). Although the idea was presented, the authors admitted the lack of experimental evidence to transform the speculations into a robust argument. Later in 1999, these motions were observed and characterized as 'Very Large Scale Motions (VLSMs)' in turbulent pipe flows by Kim & Adrian (1999), after organized motions as large as 12-14 pipe radii were observed. A detailed spectral analysis of these motions was later presented by del Álamo & Jiménez (2003) to identify their localities within the different regions of a turbulent channel boundary layer. Using two-point anchored spatial correlation functions computed over stereo PIV data, Ganapathisubramani (2005) showed the presence of these long meandering structures in the log layer of the boundary layer. That same year, the periodicity and spanwise separation of these large, ordered motions was studied using spatial correlation functions and spectral analysis by Hutchins *et al.* (2005). To separate the terminology between wall-bounded flows and turbulent boundary layer flows, Hutchins *et al.* (2005) used the term 'superstructures' specifying it for boundary layer flows.

Similarly, the presence of streamwise oriented coherent motions over various types of rough surfaces has been explored in the past. However, disagreements still exist over the region of influence where the topography of the surface dominates the flow. This region, often termed as the roughness sublayer was theorized to be confined to a wall-normal height of 3-5 k_s by Flack *et al.* (2005), where k_s is the equivalent sand grain roughness. Wu & Christensen (2010) observed qualitative consistency in statistics while comparing smooth and rough walls using flow-aligned, wall-normal PIV measurements with a scale separation of $\delta/k_s = 48$. However, a reduction in the spatial extent of coherence in the streamwise velocity was observed. Mejia-Alvarez & Christensen (2013) conducted statistical analysis of the high and low momentum regions observed in a wall-parallel, flow-aligned PIV measurement and observed similar shortening of the extent of coherence in streamwise velocity. However, a surprising streamwise elongation of the wall-normal velocity coherence was observed which was attributed to the near-wall ejections of low-momentum fluid. More recently, a somewhat contrasting observation was made by Barros & Christensen (2019) where shortening in the streamwise velocity correlations was observed for the rough-wall case, but no effect was reported on the other two velocity components.

This study aims to explore the effects of the wall roughness on the large-scale motions in the boundary layer, particularly within the roughness sublayer ($y/k_s = 2.8$) and then separately in the log-layer ($y^+ = 250$) of the smooth-wall boundary layer. Experiments for both smooth and rough configurations are presented at a Reynolds number of $1.3 \times 10^6 m^{-1}$ and at a small favourable pressure gradient. Such a study can help determine the region of influence that the homogeneously distributed roughness may have on the presence of streamwise oriented coherent structures, and reveal their connections to the low-wavenumber wall pressure fluctuations.

EXPERIMENTAL SETUP

Stability Wind Tunnel

The experiments were conducted at the Virginia Tech Stability Wind Tunnel, which is a subsonic, closed-circuit, suction-type wind tunnel. The details of the facility have been documented in Butt *et al.* (2023). The facility's port-side-wall boundary layer was tripped using a 3.18 mm tall, zig-zag shaped (internal angle of 27.6°) strip mounted in the contraction, 3.58 m upstream of the streamwise coordinate origin. A NACA 0012 airfoil (chord length = 0.914 m) was installed in the middle of the test section, such that the leading edge was 3.22 m downstream of the origin in the streamwise (X) direction at an angle of attack, $\alpha = 0°$ spanning from the floor to the ceiling. This α variation is used to manipulate the pressure gradient experienced on the side walls. As stated earlier, the current study shows results from a small pressure gradient that corresponds to $\alpha = 0°$ (details provided in Table 1).

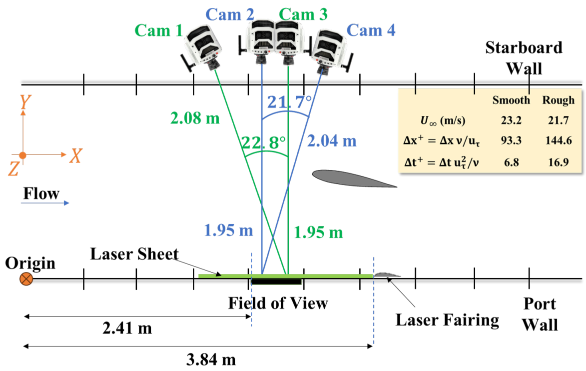

Figure 1: Experimental setup for PIV measurements

The port wall of the test section was instrumented with a high-speed laser, while the starboard wall was equipped with four high-speed cameras aimed at the measurement location (starting from X = 2.41 m) on the port wall. This location was also instrumented with an indigenously developed pressure-sensing array, capable of isolating the low-wavenumber wall-pressure fluctuations as discussed by (Damani *et al.*, 2024).

In addition to the measurements over smooth surfaces, the test section was configured by installing a k-type rough surface, extending from the origin, and spanning the entirety of the port wall, to allow comparative measurements. The rough surfaces consist of staggered cylinders of diameter $d =$ 3.14 mm, height $k_g = 2$ mm, and separated with a pitch of $s = 6.93$ mm. Vishwanathan *et al.* (2023) showed the effective sand-grain roughness of this surface to be $k_s/k_g = 1.6$. The roughness Reynolds number for the current conditions was $k_s^+ \approx 210$, which indicates the flow to be fully rough. The boundary layer growth was kept consistent with that of the smooth wall for the first 3.22 m, after which the rough surfaces were introduced. Although the location of the boundary layer's trip and airfoil α was kept consistent with the smooth-wall data, a difference in boundary layer parameters is reported in Figure 2 and Table 1.

Stereoscopic Particle Image Velocimetry

Four high-speed cameras (Phantom v2512) were used to acquire multiple sets of 24,000 time-resolved image-pairs in dual-frame mode. These cameras were mounted in a linear-configuration at a nominal working distance of 1.98 m from the plane of measurement, such that only Cam 1 and 4 housed a Scheimpflug adapter. All cameras were equipped with Nikon lenses (focal length of 200 mm each), and were installed in such a way that the resultant Field of View (FOV) created two pairs of overlapping stereoscopic planes. A pictorial representation of the camera configuration in the test section has been provided in Figure 1.

The two pairs of cameras had an 24% of overlap, which provided sufficient pixel area to stitch the two FOVs, giving a total FOV of 540 × 180 mm ($7.8\delta \times 2.6\delta$ for smooth and $5.3\delta \times 1.8\delta$ for rough case). Data was acquired at 5 kHz for smooth and 4.5 kHz for rough wall case, and processed using a commercially available software DaVis 10 distributed by LaVision. Such a configuration provided a pixel resolution of 3.58 pixels per millimeters. The spatial resolution was then enhanced using overlapping correlation windows in multiple passes of vector processing. Two initial passes of a 1:1 square window with a 50% overlap was used, followed by 3 passes of 1:1 circular window with a 75% overlap, providing a resultant vector resolution of 2.2 mm for both smooth and rough wall cases. The data acquired over the rough surfaces also underwent an additional anisotropic denoising operation to improve the SNR of the data, which was not needed for the data over smooth surfaces. The analysis presented in this study was averaged over three independent datasets from the smooth wall (total sampling time $T_s = 14.3s$) and one dataset from rough wall case ($T_s = 5.3s$).

The Boundary Layer: Smooth vs Rough Wall

Using a rake of 30 Pitot-probes housed within an aerodynamic fairing (NACA0012-34 profile, chord = 42.5 mm), the boundary layer profile for both wall configurations was measured within the FOV ($X = 2.64$ m). Figure 2, shows the boundary layer profiles for both the smooth (solid lines) and the rough (dashed lines) walls. The line style will be kept consistent to differentiate the results between rough and smooth walls for all figures throughout this paper.

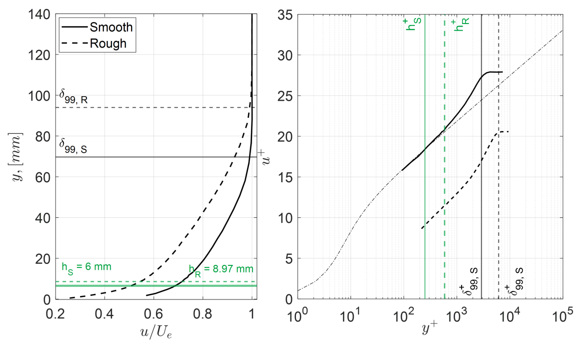

Figure 2: Boundary layer profiles for the smooth-wall (solid) and the rough-wall (dashed) cases

The green horizontal lines indicate the location of the PIV measurement plane in reference to the wall. Moreover, the black horizontal lines indicate the respective boundary layer thickness for the two surfaces. These are normalized on inner-wall units (h^+ and δ_{99}^+) and shown as vertical lines in the plot to the right of Figure 2.

Table 1: Characteristic Boundary Layer Parameters

Property	Smooth	Rough
Friction velocity Re, Re_τ	3320	6130
Momentum Re, Re_θ	9860	16970
Edge Velocity, U_e	22.7 m/s	23.9 m/s
Viscous Lengthscale, ν/u_τ	24.0 μm	15.3 μm
Clauser Parameter, β	-0.31	-0.16
Boundary Layer Thickness, δ	69.7 mm	94.0 mm
Displacement Thickness, δ^*	10.4 mm	19.5 mm
Shape Factor, H	1.40	1.51

As expected, the presence of roughness shifts the logarithmic layer of the boundary layer to the bottom and right from the smooth wall boundary layer Schetz & Bowersox (2011). A greater momentum deficit near the wall and a thicker boundary layer is observed for the rough wall. At the same flow speed, the boundary layer is approximately 25% thicker for the rough wall. Moreover, the estimated skin-friction coefficient is twice as much for the rough wall compared to the smooth wall. Further details of the boundary layer parameters are tabulated in Table 1. A doubling in Re_τ is reported here due to a 42% increase in friction velocity u_τ. On the other hand, the viscous length scales experience a 36% reduction in the presence of surface roughness.

RESULTS AND DISCUSSION

Time-resolved wall-parallel stereoscopic PIV data acquired for the two wall configurations discussed in the previous section is presented here. The smooth-wall PIV data is acquired within the log-layer ($y^+ = 250$) while that for the rough surface is acquired at a scaling of $\delta/k_s \approx 30$ at a wall-normal height of $y = 2.8k_s$ ($y^+ \approx 586$), placing the measurements in the mid-to-upper edge of the roughness sublayer. It is important to acknowledge the presence of a small to mild favourable pressure gradient in the measurement plane (i.e., β = -0.31 for smooth and β = -0.16 for rough wall). Figure 3 shows the absolute variation of the time-averaged velocity components with x (streamwise distance within the FOV) for increasing number of samples, N. Here, the deviation in the streamwise component $\Delta\overline{U}$ is shown in black, while that in the wall-normal component $\Delta\overline{V}$ is shown in red, and the spanwise $\Delta\overline{W}$ shown in blue. The colours are kept consistent for all future plots. Note that the deviation is calculated with respect to the dataset with the largest number of image-pairs, i.e., $N = 71500$.

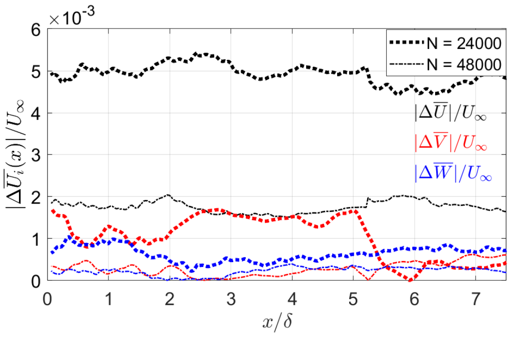

Figure 3: Absolute deviation in the time-averaged velocity components with increasing number of samples N over the smooth-wall

Figure 3 shows that the increasing number of samples used for the analysis significantly impact $\overline{U}$, suggesting the lack of convergence mostly in the streamwise component, even for a total sampling period of 14.3 s, equivalent to sampling over 3400δ flow through times. Although the deviation in the resultant mean decreases for the other two components with increasing N, the impact is significantly smaller. This is also seen in higher-order statistics presented in Figure 4 where a lack of convergence in the streamwise component of velocity can be clearly seen. Figure 4 shows the integral length scales in the streamwise direction $L_{ix}(z/\delta)$ on the left plot while integral timescales $T_{uu}(x/\delta, z/\delta)$ are shown on the right.

First, the convergence in the v and w components is achieved much faster as a direct consequence of their much shorter length and time scales. However, the u component converges slowly, varying beyond its estimated uncertainty bounds of $\pm 0.02\delta$, as the number of samples N is increased. This is an indication that events that scale on the order of several δ and extremely persisting timescales bias the results, reducing the effective number of statistically independent samples. For instance, for a total samples N of 71,500, the statistically independent samples are calculated to be $N_{eff} \approx 1500$, 25000 and 10000 for u, v and w, respectively. In other words, a streamwise oriented superstructure on the order of 20-30δ will be sampled just over 110 times in a dataset containing 71,500 samples over 14.3 s. This is of great importance, especially for efforts to computationally capture these events, as they require either an extensive domain size or impractically long simulation times. The cost and complexity of such an endeavour increases significantly once the variation of these superstructures in both space and time is taken into account, effectively deviating from the traditional Taylor's hypothesis of frozen turbulence.

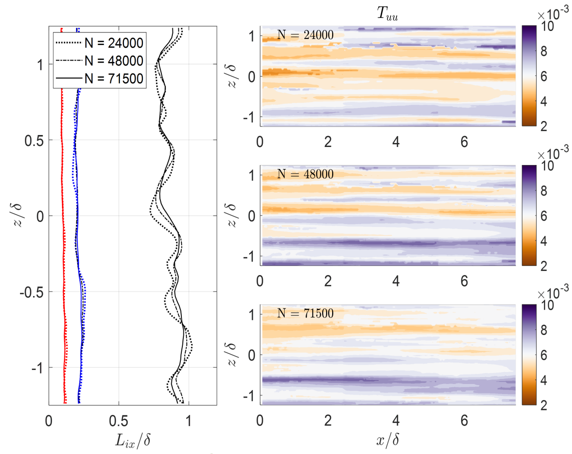

Figure 4: Integral lengthscales (left) and timescales (right) distribution over the measurement plane showing lack of convergence in u for the smooth-wall

Nevertheless, with the lack of streamwise convergence acknowledged, to understand the kinematics of the individual coherent motions within the FOV, Figure 5 shows the U_e-normalized streamwise velocity fluctuations (u) at a particular instance. The values of δ were selected for the respective wall-configuration cases, hence a difference in the δ-normalized FOV is expected.

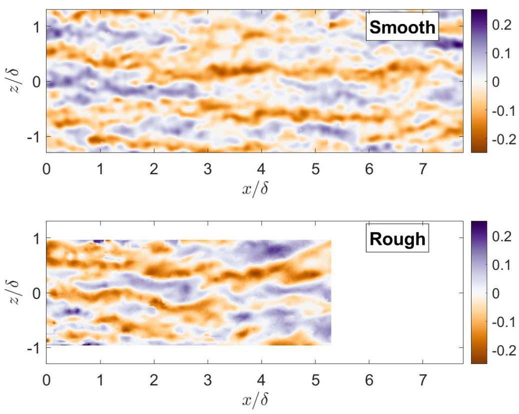

Figure 5: Instantaneous u/U_e for smooth and rough wall

Interestingly, the presence of streamwise-oriented coherent structures is visible for both smooth and rough walls at the same scaling once normalized with δ, hinting at wall-similarity at the measurement location. For both the wall configurations, the streamwise extent of the coherent motions exceeds beyond the limits of the FOV, highlighting the presence of length-scales on the order of 10δ.

To further understand the impacts of introducing surface roughness to the flow, two-point correlation coefficient functions were computed for the three velocity components discussed previously using the following relation:

$$\rho_{ab}(\Delta x, y_0, \Delta z) = \frac{\langle a(x, y_0, z, t) * b(x_0, y_0, z_0, t)\rangle}{\sqrt{a^2(x, y_0, z, t)}\sqrt{b^2(x_0, y_0, z_0, t)}} \quad (1)$$

This provides a statistical measure of the extent to which spatial coherence can be expected for each velocity component. Figure 6 provides results obtained for both the smooth (left column) and rough wall (right column), with the correlations performed at the mid-point of the FOV as the anchor point for both cases. This corresponds to $(x/\delta, z/\delta) = (4, 0)$ for the smooth, and (2.6, 0) for the rough wall case. For each component of Figure 6, the streamwise separation is presented on the horizontal axis, while the spanwise separation is presented on the vertical axis.

It is important to acknowledge the difference in the wall-normal height of the PIV planes and the thickening of the boundary layers in the presence of surface roughness in these measurements (Figure 2). Therefore, the results are scaled on their respective δ. As observed previously by Butt *et al.* (2023), positively correlated region of ρ_{uu} at the anchor point appears sandwiched between the two negatively correlated regions in the spanwise direction, indicating the presence of streamwise oriented strips of high and low momentum regions. These streamwise strips remain correlated throughout the extent of the measurement plane, highlighting the need for an even larger spatial domain in order to truly capture the largest scales that convect within the turbulent boundary layer.

While this spanwise stacking of high and low momentum regions is observed for both the rough and smooth walls, a streamwise limitation in the ρ_{uu} contours can be clearly observed for the rough wall case. In other words, the streamwise extent to which the u component remains correlated becomes limited. This modulation in the streamwise velocity could be attributed to the presence of homogeneously distributed roughness elements, channelling the flow through their spacing, restructuring the streamwise momentum, and encouraging increased spanwise meandering of the coherent superstructures in the presence of rough walls.

On the other hand, the contours of ρ_{vv} show a different outcome. While the correlated region for the smooth wall remains limited to small Δx separations, it expands for the rough wall in both the streamwise and spanwise directions. One could attribute this behaviour to the redistribution of the streamwise momentum in the wall-normal ejections of the flow, however, as indicated previously, the significantly smaller scales of the $v-$velocity subjects it to increased spatial filtering, as the spatial resolution becomes comparable at these scales. Moreover, the additional denoising operation implemented for the rough wall data tends to suppress sudden variations in the signal, effectively merging sharp boundaries of the contours and increasing their spread. While this concern remains unaddressed in the present study, the indicated restructuring relative energy of the velocity components remains a valid observation, as it is also supported by Mejia-Alvarez & Christensen (2013). Interestingly, no significant impacts of surface roughness are experienced for ρ_{ww}.

Parts of Figure 6 (such as the excellent collapsing of ρ_{ww} in both x and z, the similarity of ρ_{uu} and ρ_{vv} in the spanwise direction), provide important evidences to support the self-similarity hypothesis between smooth and homogeneously distributed rough walls, at least at the region of the boundary layer presented in this study. However, the limitations in the streamwise momentum counter this evidence by claiming the anisotropic nature of such a flow. In any case, these results provide insight to the nature of streamwise oriented superstructures that are hypothesized to excite surface pressure fluctuations.

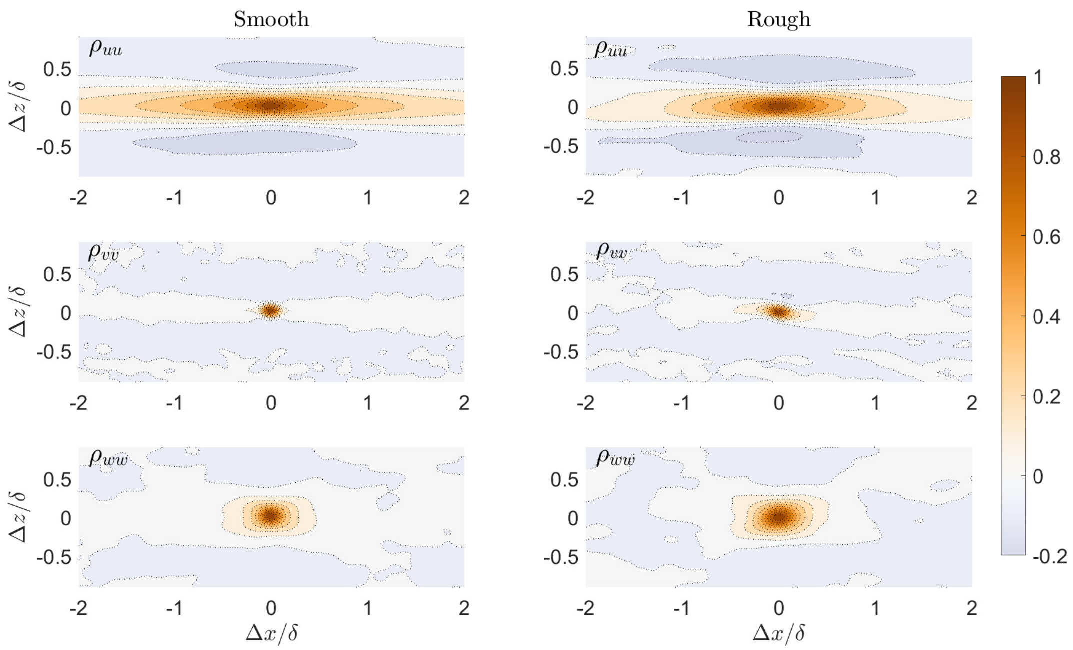

Figure 6: Two-point auto-correlation coefficient anchored at $(x,z)/\delta = (4,0)$ for smooth and $(2.6,0)$ for rough surface: ρ_{uu} (top), ρ_{vv} (middle), ρ_{ww} (bottom).

To further explore this, correlation coefficient functions for a line along the midspan of the FOV are presented in Figure 7. The streamwise clipping of ρ_{uu} for the smooth wall, and an excellent collapse of ρ_{ww} between the smooth and rough wall remain an unremarkable observation. However, the increased width of ρ_{vv} for the rough wall to the extent that it matches the spanwise component remains interesting. On the other hand, the sharp drop in the correlation at small streamwise separations for the smooth wall ρ_{vv} could clearly be attributed to the limitation of the spatial resolution at hand.

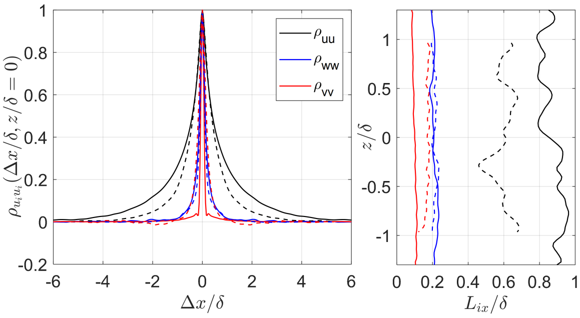

Figure 7: Left: comparisons of $\rho_{u_iu_i}$ along the mid-span line for smooth (solids) and rough (dashed) wall. Right: comparison of the integral length scales

The integral length scales along the streamwise direction L_{ix} allows a generalization of the energy organization in various velocity components in the flow as a function of their respective boundary layer thickness. The plot in the right-side of Figure 7 shows the integral length-scales of the three velocity components as a function of spanwise location, normalized on δ. The diminishing effect on the streamwise oriented coherence and enhanced wall-normal scales is another indication of the redistribution of energy in the presence of surface roughness. Moreover, the absence of statistical convergence in the streamwise velocity remains a source of uneven distribution of the higher order statistics for both rough and smooth wall. It is also important to note that the spanwise inhomogeneity of the flow was also questioned before confidently attributing the results predominantly to the lack of convergence. However, this specific analysis is not presented here for brevity.

While the single and two-point statistics are discussed in some detail, it is important to argue the value of such an analysis in the context of their contributions to inducing surface pressure fluctuations, as that is the core motivation for this study. As discussed earlier, the contribution of superstructures, or their consequential influence on other near-wall flow phenomenon is hypothesized to be responsible for inducing convective, and more interestingly, the sub-convective wall pressure fluctuations. This connection between the pressure fluctuations and their sources are given by the pressure Poisson's equation given as:

$$\frac{1}{\rho}\nabla^2 p = -2\frac{\partial u_j}{\partial x_i}\frac{\partial U_i}{\partial x_j} - \frac{\partial^2}{\partial x_i \partial x_j}(u_i u_j - \overline{u_i u_j}) \qquad (2)$$

The details of the terms involved in Equation 2, along with the difficulty in their experimental measurements are discussed extensively by Blake (2017). While recent studies have argued for the relative importance of both the rapid (first term in Equation 2) and slow (second term) terms, their experimental verification remains a challenge, even for the rapid term which is assumed to be the simpler of the two due to its linearity. Although this requires a comprehensive volumetric flow measurement in synchrony with wall-pressure measurements, the current study remains limited to a sheet of velocity measurements at a certain wall-normal height from the surface. Nevertheless, the cross-coherence of velocity fluctuation terms can, at this point, reveal their relative importance, and drive future research to quantify individual source terms of the pressure-Poisson's equation. For that, cross-correlation coefficient functions of the three velocity components are plotted in Figure 8. The axis, as well as the anchor points, are kept consistent with those presented earlier in Figure 6. Interestingly, the contours of ρ_{uv} exhibit the same nature as that by ρ_{uu}, albeit with an opposite sign. The negative sign could be attributed to the direction of the wall-normal velocity that remains correlated with u, spanning almost the entirety of the FOV. This nature, with a stronger magnitude is seen for the rough wall case as well. This increased strength in the correlation can be attributed to the increased coherence seen in the contours of ρ_{vv}. The relatively disturbed nature of the correlations contours for the rough wall also suggests the need for including more averages to better converge the higher order statistics involving u.

The other two cross-terms: ρ_{uw} and ρ_{vw} exhibit a dipolar nature in their correlations, sourcing outwards from the anchor point in the flow direction, with the former having a relatively stronger impact. This region of correlation is relatively smaller than that of ρ_{uu} and ρ_{uv}, but interestingly is significantly larger than ρ_{vv} and ρ_{ww}, indicating the importance of carefully resolving the cross-correlation terms in future studies. In other words, the inclusion of the slow term, specifically the uv and uw components, in order to relate the velocity sources to the surface pressure fluctuations more accurately, is arguably as important as the the rapid term. On the other hand, while the contours of ρ_{vw} may appear relatively weak compared to the other terms, the modulation of this component remains important to the study of wall-pressure fluctuations over rough surfaces. In conclusion, the results presented here highlight the relative importance of each of the velocity source terms that contribute to the generation of surface pressure fluctuations, and provide a foundation for future experimental campaigns.

CONCLUSION

Wall-parallel stereoscopic PIV measurements were conducted over smooth and k-type rough surfaces using a large FOV to capture the streamwise oriented coherent motions within a turbulent boundary layer at $Re/m = 1.31 \times 10^6$, and at $y^+ \approx 250$ and 580 for smooth and rough walls, respectively. For a fully rough flow ($k_s^+ \approx 210$) and a roughness scaling of $\delta/k_s \approx 30$, the streamwise extent of the superstructures experienced shortening when compared to the smooth wall. However, a reorganization of streamwise momentum into the wall-normal component was observed upon the introduction of roughness, whereas the w component experienced minimal effects in the presence of surface roughness. The need for increased sampling was highlighted to accurately capture the streamwise oriented superstructures and their impacts on near-wall flow phenomena, by showing the lack of convergence in the two-point statistics of the flow. It was found that a sampling of over 3400 boundary layer flow through times was inadequate to quantify the largest scales with increased statistical confidence.

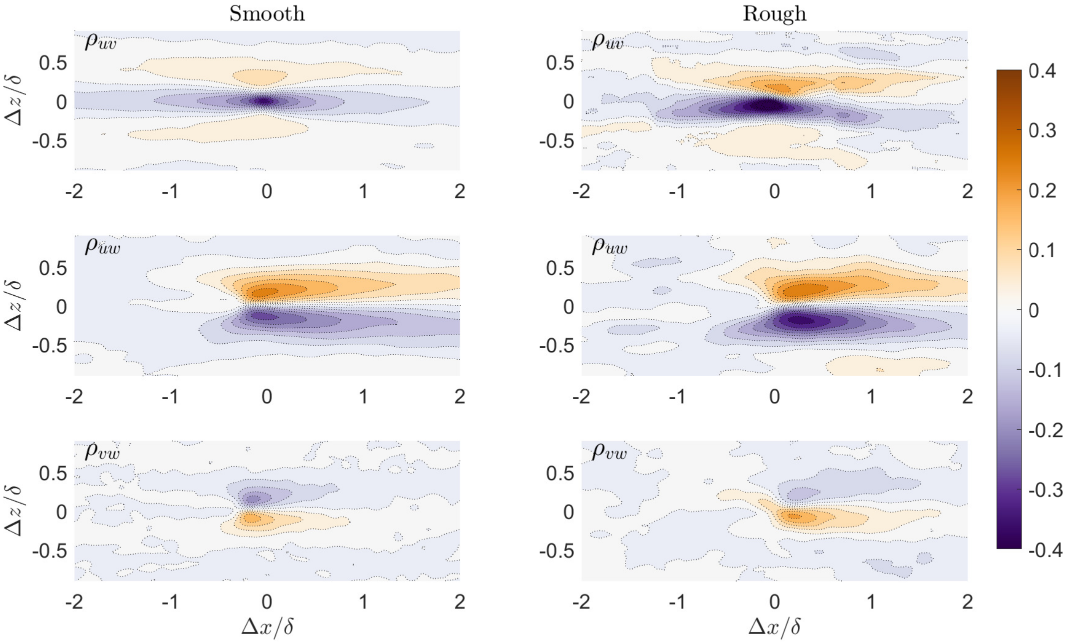

Figure 8: Two-point cross-correlation coefficient anchored at $(x,z)/\delta = (4,0)$ for smooth and $(2.6,0)$ for rough surface: ρ_{uv} (top), ρ_{uw} (middle), ρ_{vw} (bottom).

The extent of ρ_{uv} spanning the entire FOV and sizeable magnitudes of ρ_{uw} revealed the significance of the slow terms in the pressure Poisson equation. This highlighted the importance of the *uv* and *uw* components, over the traditionally assumed linear (or rapid) terms, in the quantification of source terms of the low-wavenumber surface pressure fluctuations with increased accuracy. However, the causal relationships of the velocity source terms and their quantitative relative contributions to low-wavenumber wall-pressure fluctuations remain a topic of interest for future studies.

ACKNOWLEDGEMENTS

The authors would like to thank Dr. Yin-Lu Young and the Office of Naval Research (ONR) for sponsoring this research under grant numbers N00014-20-1-2821 and N00014-22-1-2789. The authors would also like to acknowledge the efforts of the machine shop at the AOE department at Virginia Tech, and the staff at the VT Stability Wind Tunnel.

REFERENCES

del Álamo, Juan C. & Jiménez, Javier 2003 Spectra of the very large anisotropic scales in turbulent channels. *Physics of Fluids* **15** (6), L41.

Barros, Julio M & Christensen, Kenneth T 2019 Characteristics of large-scale and superstructure motions in a turbulent boundary layer overlying complex roughness. *Journal of Turbulence* **20** (2), 147–173.

Blake, William K 2017 *Mechanics of flow-induced sound and vibration, Volume 2: Complex flow-structure interactions*. Academic press.

Butt, Humza, Damani, Shishir, Srivastava, Surabhi, Chaware, Shreyas S, Szoke, Máté, Devenport, William J, Lowe, Todd, Hales, Alistair, Colbrook, Matthew & Ayton, Lorna J 2023 Pressure gradient effects on boundary layer superstructures. In *AIAA AVIATION 2023 Forum*, p. 3337.

Damani, Shishir, Totten, Eric, Butt, Humza, Sharma, Bhavika, Devenport, William J. & Lowe, Todd 2024 The nature of turbulent boundary layer sub-convective pressure fluctuations. In *13th International Symposium on Turbulence and Shear Flow Phenomena (TSFP13)*.

Flack, Karen A, Schultz, Michael P & Shapiro, Thomas A 2005 Experimental support for townsend's reynolds number similarity hypothesis on rough walls. *Physics of Fluids* **17** (3).

Ganapathisubramani, B. et al. 2005 Investigation of large-scale coherence in a turbulent boundary layer using two-point correlations. *Journal of Fluid Mechanics* **524**, 57–80.

Hutchins, Nick, Ganapathisubramani, Bharath & Marusic, Ivan 2005 Spanwise periodicity and the existence of very large scale coherence in turbulent boundary layers. In *Fourth International Symposium on Turbulence and Shear Flow Phenomena*. Begel House Inc.

Kim, K. C. & Adrian, R. J. 1999 Very large-scale motion in the outer layer. *Physics of Fluids* **11** (2), 417–422.

Kovasznay, L S G 1970 The turbulent boundary layer. *Annual Review of Fluid Mechanics* **2** (1), 95–112.

Mejia-Alvarez, Ricardo & Christensen, Kenneth 2013 Publisher's note: "wall-parallel stereo particle-image velocimetry measurements in the roughness sublayer of turbulent flow overlying highly irregular roughness" [phys. fluids 25, 115109 (2013)]. *Physics of Fluids* **25**, 115109.

Schetz, Joseph A & Bowersox, Rodney DW 2011 *Boundary layer analysis*. American Institute of Aeronautics and Astronautics.

Vishwanathan, Vidya, Fritsch, Daniel J., Lowe, K. Todd & Devenport, William J. 2023 History effects and wall-similarity of non-equilibrium turbulent boundary layers in varying pressure gradient over rough and smooth surfaces. *International Journal of Heat and Fluid Flow* **102**, 109145.

Wu, Y. & Christensen, K. T. 2010 Spatial structure of a turbulent boundary layer with irregular surface roughness. *Journal of Fluid Mechanics* **655**, 380–418.